Numerical Solution of a Two Component Reaction-Diffusion Equation in Two Spatial Dimensions

by

John N. Homenuke

A THESIS SUBMITTED IN PARTIAL FULFILMENT OF
THE REQUIREMENTS FOR THE DEGREE OF

Bachelor of Science

in

The Faculty of Science

(Physics)

The University Of British Columbia

April 21, 2006

Abstract

This work details the solution to a two component reaction-diffusion equation known as the classical Gierer-Meinhardt model in (2+1) dimensions using Crank-Nicholson and nonlinear multigrid methods. Stripe initial conditions are examined in one of two distinct interaction regimes, the weak interaction regime, which display breakup instabilities for certain parameter spaces.

Table of Contents

List of Figures

Acknowledgements

Much thankfulness goes to my supervisor Matthew Choptuik for providing the opportunity to take my education as far as it has gone, to everyone in the Numerical Relativity group for their assistance in problem solving, but most of all to the Lord for His seemingly endless grace throughout this project.

Chapter 1

Introduction

1.1 Biological Development and Pattern Formation

The field of biology has traditionally obtained most of its knowledge of developmental control by experiment. For instance, the effect of transplantation of tissue into unnatural places during development of an embryo may be very well documented, but no underlying mechanism for predicting the changes is provided [4]. Whereas in other fields of science such as physics, mathematically formulated theories are used extensively which yield quantitative solutions that sometimes precede experimental discovery.

Biological development proceeds using genetic material as a recipe of sorts, but this does not explain differentiation in tissue because the genetic material is the same in most cells of an organism. Embryos of certain species can be split after their first division to form two independent embryos. So the full structure of the adult organism cannot be contained in the original cell and the final form must be generated from less complex tissue through an internal regulatory process [4]. New features in an organism can be formed by a number of possible mechanisms termed by Meinhardt as organizing

centres, inhibitory fields, polarity, and prepatterns. In this case, we will examine so-called "morphogenic" fields where localized high concentrations of a morphogen are formed that then provide a blueprint for the development of these new biological features.

In 1952, Turing [5] discovered (mathematically) that an interaction of two chemical morphogens with different diffusion rates in a reaction-diffusion model could create patterns of high and low concentration. He was forced to use the linearized equations because of difficulty in solving the full non-linear case, but suggested a digital computer would be useful in that process. His solutions to the linearized case turned out to be unstable, but it was later shown that his nonlinear equations returned steady-state, periodic distributions [3]. Intuitively one expects that diffusion would spread both components into ultimately uniform concentrations. Instead we find localized autocatalysis and cross catalysis occurring amidst long-range inhibition. This suggests that a dynamical, stable relationship can exist between two chemicals and cause patterned growth in biological systems.

A pattern is formed when spatial differencing occurs in a roughly uniform field. The question is how does this pattern arise from seemingly little information? There are many non-living processes in nature that feedback on themselves such as the creation of sand dunes or the winding of a river through a valley. Only small deviations are needed to initiate growth into much larger phenomena. There must also be a competing effect in order to create a pattern. If sand is deposited on a dune or the inside curve of a river then it must be eroding from the surroundings. The pattern is dictated by the relative strength of the these two forces at every point in the field and

furthermore the growth of the pattern depends on its present state. Thus we can envision a model represented by a system of differential equations.

1.2 Activator-Inhibitor Systems

The model examined here is a hypothetical biochemical reaction assumed to take place in a developing organism. Let there be two components, one called an activator with concentration a and the other an inhibitor with concentration h. The activator's duty is to initiate some other biochemical process needed for development of the organism. The activator undergoes autocatalysis to effect local growth of small deviations, but is also consumed by the inhibitor. The reaction kinetics are such that the activator will outpace the inhibitor growth given a high enough concentration ratio of the two, but the inhibitor will suppress the activator in the outlying regions where there is little activator. The inhibitor is designed with a faster diffusivity. This maintains global stability of the entire system by spreading it uniformly over the domain and allows the activator to form regions of relatively high and low concentrations. The diffusion of the activator ultimately keeps it from growing out of control, leading to a steady-state pattern. This provides the organism with positional information An example is as follows.

$$\frac{\partial a}{\partial t} = D_a \frac{\partial^2 a}{\partial x^2} - \mu a + \frac{a^2}{h} \tag{1.1}$$

$$\frac{\partial h}{\partial t} = D_h \frac{\partial^2 h}{\partial x^2} - \nu h + a^2 \tag{1.2}$$

The linear reaction terms are a simple assumption that the rate that molecules escape from the system depends linearly on how many are present. Turing

[5] found that this type of system can organize itself into a field of regularly spaced spots whose qualitative features depended little on the initial conditions.

1.3 Gierer-Meinhardt Model

The above system can be generalized to different exponent sets (p, q, r, s) in the Gierer-Meinhardt model written here in non-dimensionalized form

$$\frac{\partial a}{\partial t} = {\epsilon_0}^2 \nabla^2 a - a + \frac{a^p}{h^q} \tag{1.3}$$

$$\tau \frac{\partial h}{\partial t} = D\nabla^2 h - h + \frac{a^r}{\epsilon_0 h^s}. \tag{1.4}$$

This system will be solved on a rectangular domain

$$\mathbb{X} = \{(t, X, Y) : t \geq 0, -1 \leq X \leq 1, 0 \leq Y \leq d_0\} \tag{1.5}$$

with Neumann conditions $\partial_n a = \partial_n h = 0$ on the boundary. The exponent set (p, q, r, s) satisfies

$$\frac{qr}{p-1} - (s+1) > 0, \quad p > 1, \quad q > 0, \quad r > 1, \quad s \geq 0. \tag{1.6}$$

1.4 Stripe Solutions and their Stability

The initial conditions examined herein are equilibrium stripe solutions with small perturbations. For certain parameter ranges the stripe is unstable to these perturbations and subsequently displays two distinct (although often co-existing) phenomena: spot formation and zigzag formation.

There are two interaction regimes defined by the relative diffusivities of the two components. In the *semi-strong* regime, $\epsilon_0 \ll 1$ and $D = O(1)$,

making the ratio of diffusivities asymptotically large. In such case, one of the solution components becomes localized, while the other spreads over the whole domain very quickly. In the *weak* interaction regime, $\epsilon_0 \ll 1$ and $D = D_0{\epsilon_0}^2 \ll 1$. Here, both components become localized and interact negligibly with the domain boundaries and neighbouring stripes.

This work details the code for the numerical simulations of (1.3) and will compare the outcome expected from the stability analysis in the weak interaction regime with those simulations.

Chapter 2

Stability Analysis

To initialize our solutions in the weak interaction regime as was done in [2], we need homoclinic equilibrium solutions to (1.3). We set the time derivitives to zero and re-scale a, h, and $X = x/l$, $D = D_0{\epsilon_0}^2$ to get the system

$$\frac{\partial^2 a}{\partial x^2} - a + \frac{a^p}{h^q} = 0, \quad D_0\frac{\partial^2 h}{\partial x^2} - h + \frac{a^r}{h^s} = 0 \tag{2.1}$$

The solutions to this are 1-dimensional stripe cross-sections. This was done using the DE solver `dsolve` with method `BVP` in Maple 8 on a domain $l = 15.0$. Figure 2.1 plots the central maximum $a(0)$ of these solutions versus D_0.

Let these solutions be labelled a_e and h_e. We can then write the ansatz

$$\begin{aligned} a &= a_e(x/\epsilon_0) + \Phi(x/\epsilon_0)e^{\lambda t}\cos(my), \\ h &= h_e(x/\epsilon_0) + N(x/\epsilon_0)e^{\lambda t}\cos(my), \end{aligned} \tag{2.2}$$

to determine the stability along the branch in figure 2.1. Substituting (2.2) into (1.3) returns an eigenvalue problem,

$$\begin{aligned} \Phi_{zz} - (1+\mu)\Phi + \frac{p{a_e}^{p-1}}{{h_e}^q}\Phi - \frac{q{a_e}^p}{{h_e}^{q+1}}N &= \lambda\Phi, \\ D_0 N_{zz} - (1+D_0\mu)N + \frac{r{a_e}^{r-1}}{{h_e}^s}\Phi - \frac{s{a_e}^r}{{h_e}^{s+1}}N &= \tau\lambda N, \end{aligned} \tag{2.3}$$

where $z = x/\epsilon_0$ and $\mu = {\epsilon_0}^2 m^2$. From this, one can numerically determine the range of μ and D_0 that contain real, positive eigenvalues λ. The type

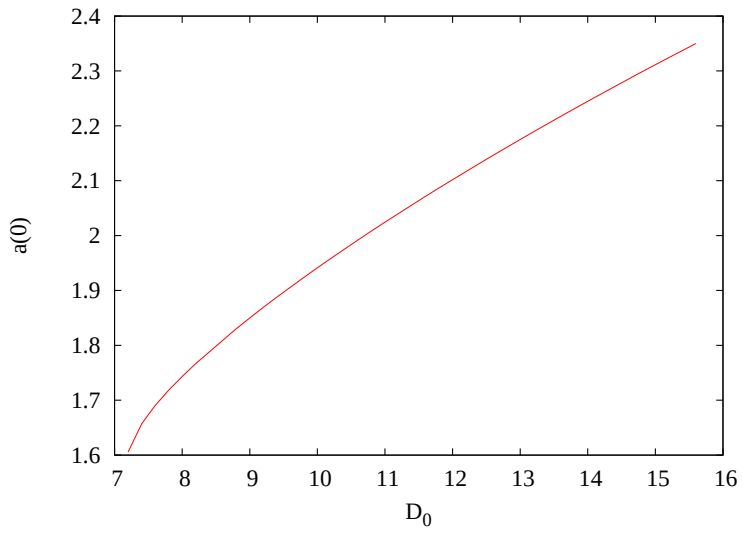

Figure 2.1: Upper branch of bifurcation diagram of central maximum $a(0)$ versus D_0 for the solution to (2.1) with exponents $(p, q, r, s) = (2, 1, 2, 0)$.

of instability depends on the form of the eigenfunctions Φ and N. Breakup instabilities occur for even eigenfunctions and zigzag instabilities for odd eigenfunctions.

Chapter 3

Numerics

Most systems of nonlinear PDEs have no closed-form solutions that can be found by hand. Rather, we need a numerical approximation of the solution. Finite-difference techniques are implemented here that approximate the domain and the solution with a set of grid points. A good numerical scheme will converge to the exact solution of the system in the limit that the spacing between the points $h \to 0$.

3.1 Finite-difference Approxmiations and Numerical Analysis

We begin by discretizing the domain

$$\mathbb{X} = \{(t, x, y) : t \geq 0, 0 \leq x \leq 1, 0 \leq y \leq 1\}. \tag{3.1}$$

Let there be $N = 2^l + 1$ points along the x and y axes, where $l \in \mathbb{Z}^+$, for a total of N^2 spatial points. The distance $h = 1/(N-1)$ between these points is called the mesh spacing. The spacing in the time dimension Δt is defined by the Courant number λ where $\Delta t = \lambda h$. Typically this number is constrained to $0 < \lambda < 1$. If we index the points by the integers (i, j, n),

then we can write the discrete domain as

$$\mathbb{X}_h = \{(t^n, x_i, y_j) : t^n = n\Delta t, x_i = (i-1)h, y_j = (j-1)h\}. \tag{3.2}$$

3.1.1 Error Analysis

Let the exact, continuous solution be $u = u(t, x, y)$. The numerical solution is

$$\hat{u} = u_{i,j}^n = u(t^n, x_i, y_j) + \hat{e} \tag{3.3}$$

where $\hat{e}$ is the solution error.

What is left now is to discretize the system of equations we want to solve. Let the continuum system be represented as

$$\mathcal{L}(u) = 0 \tag{3.4}$$

and the discrete system be represented as

$$\hat{\mathcal{L}}(\hat{u}) = 0. \tag{3.5}$$

The truncation error is defined as

$$\hat{\tau} \equiv \hat{\mathcal{L}}(\hat{u}) - \hat{\mathcal{L}}(u). \tag{3.6}$$

It can be shown that $O(\hat{e}) = O(\hat{\tau})$, placing bounds on the solution error for a given truncation error. As an example from [1], consider the simple system

$$\frac{d}{dx}u(x) = u(x) \tag{3.7}$$

whose solution is $u(x) = e^x$. Let us apply the scheme

$$\frac{u_{i+1} - u_i}{h} = \frac{u_{i+1} + u_i}{2} \tag{3.8}$$

which uses the difference operators

$$\begin{aligned} \Delta_x u_i &= \frac{u_{i+1} - u_i}{h}, \\ \mu_x u_i &= \frac{u_{i+1} + u_i}{2}. \end{aligned} \tag{3.9}$$

This scheme is very similar to the Crank-Nicholson scheme discussed below and is "naturally centred" about the point $i + 1/2$. So consider the Taylor expansions of the solutions about the point $i + 1/2$.

$$u_{i+1/2} = \bar{u} = u(x_i + h/2) \tag{3.10}$$

$$u_{i+1} = \bar{u} + \left(\frac{h}{2}\right)\bar{u}' + \frac{1}{2}\left(\frac{h}{2}\right)^2\bar{u}'' + \frac{1}{6}\left(\frac{h}{2}\right)^3\bar{u}''' + O(h^4) \tag{3.11}$$

$$u_i = \bar{u} - \left(\frac{h}{2}\right)\bar{u}' + \frac{1}{2}\left(\frac{h}{2}\right)^2\bar{u}'' - \frac{1}{6}\left(\frac{h}{2}\right)^3\bar{u}''' + O(h^4) \tag{3.12}$$

Substituting these into (3.9), we get the error associated with the operators,

$$\begin{aligned} \Delta_x u_i &= \frac{u_{i+1} - u_i}{h} = \bar{u}' + \frac{h^2}{24}\bar{u}''' + O(h^4), \\ \mu_x u_i &= \frac{u_{i+1} + u_i}{2} = \bar{u} + \frac{h^2}{8}\bar{u}'' + O(h^4). \end{aligned} \tag{3.13}$$

The operators themselves can be written as power series in h.

$$\begin{aligned} \Delta_x &= \frac{d}{dx} + \frac{h^2}{24}\frac{d^3}{dx^3} + O(h^4) \\ \mu_x &= 1 + \frac{h^2}{8}\frac{d^2}{dx^2} + O(h^4) \end{aligned} \tag{3.14}$$

We can now compute the above definition (3.6) of truncation error,

$$\mathcal{L} = \frac{d}{dx} - 1 \tag{3.15}$$

$$\hat{\mathcal{L}} = \Delta_x - \mu_x \tag{3.16}$$

$$\begin{aligned}\hat{\tau} &= \hat{\mathcal{L}}(\hat{u}) - \hat{\mathcal{L}}(u) \\ &= 0 - \hat{\mathcal{L}}(u) \\ &= \left(1 + \frac{h^2}{8}\frac{d^2}{dx^2} - \frac{d}{dx} - \frac{h^2}{24}\frac{d^3}{dx^3}\right) u \\ &= \left(1 - \frac{d}{dx}\right) u + h^2 \left(\frac{1}{8}\frac{d^2}{dx^2} - \frac{1}{24}\frac{d^3}{dx^3}\right) u \end{aligned} \tag{3.17}$$

$$\hat{\tau} = O(h^2). \tag{3.18}$$

Now assume the numerical solution has error representable as an even power series in h, a so-called *Richardson expansion*. This is reasonable if the scheme is centred.

$$\hat{u} = u + e_2 h^2 + e_4 h^4 + O(h^6) \tag{3.19}$$

Recall equation (3.5). Substituting the Taylor expanded scheme (3.14) and the expansion (3.19) results in

$$\left[\left(\frac{d}{dx} - 1\right) + h^2 \left(\frac{1}{24}\frac{d^3}{dx^3} - \frac{1}{8}\frac{d^2}{dx^2}\right) + O(h^4)\right] \left[u + e_2 h^2 + O(h^4)\right] = 0. \tag{3.20}$$

Expanding this returns

$$\left(\frac{d}{dx} - 1\right) u + h^2 \left(\frac{d}{dx} - 1\right) e_2 + h^2 \left(\frac{1}{24}\frac{d^3}{dx^3} - \frac{1}{8}\frac{d^2}{dx^2}\right) u + O(h^4). \tag{3.21}$$

We already know that $u' = u$ and assume that $h^4 \approx 0$ for our purposes. This leaves

$$h^2 \left(1 - \frac{d}{dx}\right) e_2 = h^2 \left(\frac{1}{24}\frac{d^3}{dx^3} - \frac{1}{8}\frac{d^2}{dx^2}\right) u, \tag{3.22}$$

and given that $u = e^x$, $e_2 = -xe^x/12$. Thus our solution error is

$$\hat{e} = \frac{h^2}{12} x e^x = O(h^2). \tag{3.23}$$

3.1.2 Convergence

We usually choose to solve differential equations numerically becuase we don't know the closed-form solution if it exists at all. So how can we be sure our scheme actually provides the correct answer? There are two tests one can perform. The first is a test of the convergence rate by generating at least 3 solutions using a proposed scheme with a truncation error of $O(h^p)$. Let u_h, u_{2h}, and u_{4h} be solutions with mesh size denoted by their subscripts. If

$$\frac{u_{4h} - u_{2h}}{u_{2h} - u_h} \to 2^p \text{ as } h \to 0, \tag{3.24}$$

then the scheme is said to be convergent to $O(h^p)$ as predicted. The Crank-Nicholson scheme used here has $O(h^2)$ truncation error and this is confirmed in figure 3.1. But this only confirms that it converges to the continuum solution of a system that isn't necessarily identical to the one intended. The second test is called an independent residual test in which one builds a different scheme for the same system. If the two schemes generate the same solution within truncation error, then one can be confident the true solution has been computed.

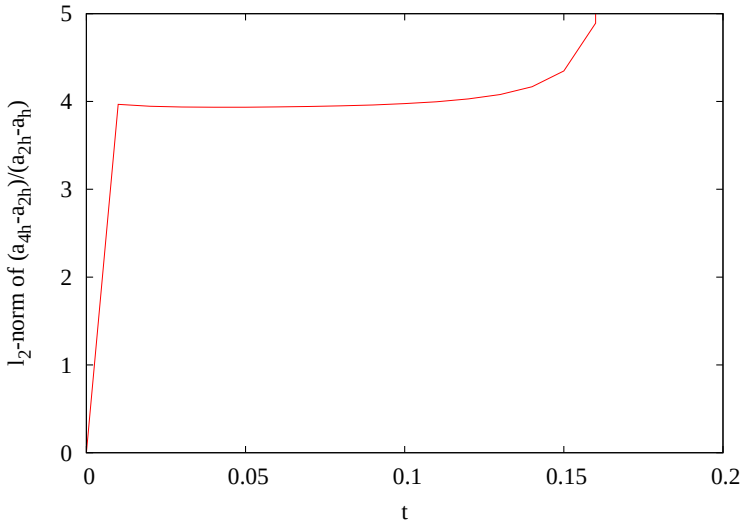

Figure 3.1: Convergence test on domain $[-0.25, 0.25] \times [0, 0.50]$ with 128×128, 256×256, and 512×512, points for their repsective grids. The scheme is $O(h^2)$ convergent only up to $t = 0.16$. Then the convergence rate essentially diverges which is not strictly speaking a loss of convergence, but it is unclear how reliable the scheme is beyond this.

3.2 Building Discrete Systems

3.2.1 Taylor Series Approximations

Next we need a method for finding a consistent and stable discrete system of equations. The basic procedure is to approximate the differential operators in the equations by difference operators using Taylor series. For example, the first derivitive is approximated by the slope between two neighbouring points. This comes about by solving a truncated Taylor series for $u'(x)$.

$$u(x+h) = u(x) + hu'(x) + \frac{h^2}{2}u''(x) + O(h^3) \tag{3.25}$$

$$u'(x) = \frac{u(x+h) - u(x)}{\Delta t} - \frac{h}{2}u''(x) + O(h^2) \tag{3.26}$$

$$\Delta_x^{\mathrm{F}}(u_i) = \frac{u_{i+1} - u_i}{\Delta t} \tag{3.27}$$

We choose only use the leftmost terms in the solution scheme. The remaining ones are dropped, hence they sum to what is called the truncation error $\hat{\tau}$. The operator $\Delta_x^{\mathrm{F}}(u_i)$ is called a forward difference operator because it uses the ith and $(i+1)$st points. Its truncation error is $O(h)$ as indicated by the leading-order error term in (3.26).

As another example, we get the centered second derivitive whose leading error term is $O(h^2)$ by using two Taylor series as follows.

$$u(x+h) = u(x) + hu'(x) + \frac{h^2}{2}u''(x) + O(h^3) \tag{3.28}$$

$$u(x-h) = u(x) - hu'(x) + \frac{h^2}{2}u''(x) - O(h^3) \tag{3.29}$$

Adding these equations, $u'(x)$ disappears and we are left with

$$u''(x) = \frac{u(x-h) - 2u(x) + u(x+h)}{h^2} + O(h^2), \tag{3.30}$$

$$\Delta_{xx}^{\mathrm{C}}(u_i) = \frac{u_{i-1} - 2u_i + u_{i+1}}{h^2}. \tag{3.31}$$

The boundary conditions are defined with the same method and have first-order accuracy. All solutions in this work are computed with Neumann conditions,

$$\begin{aligned} \frac{\partial u}{\partial x}(-l,y)=0 \quad &\rightarrow \quad \frac{u_{2,j}-u_{1,j}}{\Delta x}=0 \\ \frac{\partial u}{\partial x}(l,y)=0 \quad &\rightarrow \quad \frac{u_{N,j}-u_{N-1,j}}{\Delta x}=0 \\ \frac{\partial u}{\partial y}(x,0)=0 \quad &\rightarrow \quad \frac{u_{i,2}-u_{i,1}}{\Delta y}=0 \\ \frac{\partial u}{\partial y}(x,d)=0 \quad &\rightarrow \quad \frac{u_{i,N}-u_{i,N-1}}{\Delta y}=0 \end{aligned} \tag{3.32}$$

The domain here is $[-l,l]\times[0,d]$ discretized on a $N\times N$ grid.

3.2.2 Crank-Nicholson Scheme

The system is

$$\frac{da}{dt}=\epsilon\nabla^2 a-a+\frac{a^p}{h^q} \tag{3.33}$$

$$\frac{1}{\tau}\frac{dh}{dt}=\nabla^2 h-h+\frac{1}{\epsilon^2}\frac{a^r}{h^s}. \tag{3.34}$$

A Crank-Nicholson scheme will provide second-order accuracy in the mesh size. Since the equations are nearly identical, only one will be shown.

$$\frac{a_{i,j}^{n+1}-a_{i,j}^{n}}{\Delta t}=\frac{1}{2}\left(\nabla^2 a_{i,j}^{n+1}+\nabla^2 a_{i,j}^{n}+f(a_{i,j}^{n+1},h_{i,j}^{n+1})+f(a_{i,j}^{n},h_{i,j}^{n})\right) \tag{3.35}$$

where $f(a,h)=-a+a^p/h^q$. The Laplacians are written as

$$\nabla^2 a_{i,j}^{n}=\frac{1}{\Delta x}\left(a_{i-1,j}^{n}-2a_{i,j}^{n}+a_{i+1,j}^{n}\right)+\frac{1}{\Delta y}\left(a_{i,j-1}^{n}-2a_{i,j}^{n}+a_{i,j+1}^{n}\right) \tag{3.36}$$

with the mesh spacings written as Δx and Δy to avoid confusion with h here. The $(n+1)$ terms and (n) terms are isolated on either side,

$$\begin{aligned} a_{i,j}^{n+1}-\frac{\Delta t}{2}&\left(\nabla^2 a_{i,j}^{n+1}+f(a_{i,j}^{n+1},h_{i,j}^{n+1})\right) \\ &=a_{i,j}^{n}+\frac{\Delta t}{2}\left(\nabla^2 a_{i,j}^{n+1}+f(a_{i,j}^{n+1},h_{i,j}^{n+1})\right), \end{aligned} \tag{3.37}$$

and what is left is an elliptic equation to be solved using multigrid (MG) techniques. The MG method is run at each time step using the solution at the previous time step as an initial guess for the next.

3.2.3 Leapfrog Scheme

An alternative to the Crank-Nicholson scheme is the Leapfrog scheme. Unlike CN schemes it is only conditionally stable, but is has the advantage that it is an explicit scheme and doesn't require multiple iterations of an elliptic solver within each time step. It has its name for its basic structure:

$$\frac{\partial u}{\partial t} = f(u,t) \quad \rightarrow \quad \frac{u^{n+1} - u^{n-1}}{2\Delta t} = f(u^n, t^n). \tag{3.38}$$

The time derivitive is defined by the solution at the past and future time-steps rather than the present.

Applying this scheme to our equations here, we get

$$\frac{u^{n+1} - u^{n-1}}{\Delta t} = \nabla^2 a^n - a^n + \frac{(a^n)^p}{(h^n)^q}. \tag{3.39}$$

One can solve for a^{n+1} explicitly to determine the next time step.

3.3 Multigrid

Multigrid came into popular use in the early 80s as a means of solving elliptic equations. Traditionally they are solved by successive applications of a relaxation formula until convergence to the correct solution is achieved. This is a slow process because the convergence rate is inversely proportional to the number of points N in the domain. The advantage of multigrid is that its convergence rate is independent of N.

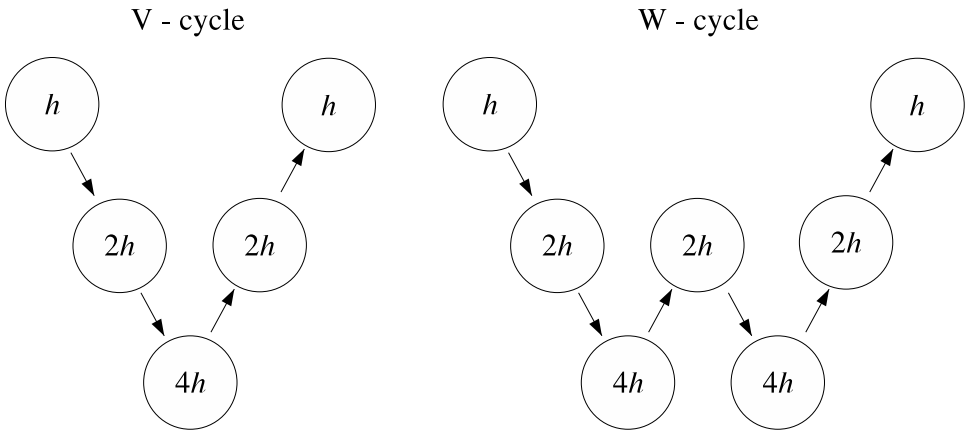

Figure 3.2: Schematic of multigrid routines. The arrows represent grid transfers and the values in the circles are the mesh sizes. The relaxation scheme is run only a few times at on each grid except for the lowest one where most of the convergence takes place.

The strategy is to transfer the temporary solution to a series of coarser grids and relaxing the solution to convergence (solving) on the coarsest grid and then to transfer it back to the original fine grid. A few relaxation sweeps (smoothing) are necessary on the intermediate grids to keep the residual (which adds "jaggedness" to the solution) relatively small. The simplest arrangement of these steps is called a *V-cycle* in which the solution is transfered successively to the coarsest grid, solved, and back to the fine grid. Alternatively, one can implement more than one V-cycle or a *W-cycle* as in figure 3.2.

There are three operations used to accomplish this:

Restriction Operator $\mathcal{R}$ Transfers the temporary solution to the next coarsest grid of mesh size twice the current one. Rather than simply

leaving out every second point, a weighted sum of the surrounding points is used.

$$\begin{bmatrix} \frac{1}{16} & \frac{1}{8} & \frac{1}{16} \\ \frac{1}{8} & \frac{1}{4} & \frac{1}{8} \\ \frac{1}{16} & \frac{1}{8} & \frac{1}{16} \end{bmatrix} \tag{3.40}$$

Prolongation Operator $\mathcal{P}$ Transfers the temporary solution to the next finest grid using a bilinear interpolation.

$$\begin{bmatrix} \frac{1}{4} & \frac{1}{2} & \frac{1}{4} \\ \frac{1}{2} & 1 & \frac{1}{2} \\ \frac{1}{4} & \frac{1}{2} & \frac{1}{4} \end{bmatrix} \tag{3.41}$$

$\mathcal{P}$ is the adjoint operator to $\mathcal{R}$.

Relaxation Scheme The scheme we choose depends on the type of system we are solving. Here we need a nonlinear relaxation scheme such as the Newton Gauss-Seidel method. Let $\mathbf{u}$ be a D-dimensional vector function of some set of space-time variables and $\mathbf{L}(\mathbf{u}) = \mathbf{f}$ represent a systems of D equations. We discretize this system on a domain of N grid points, giving us a total of DN unknowns.

The goal here is to iterate this scheme on a single point in the domain until the local residual $\mathbf{r} \to \mathbf{0}$. We do this for the D unknowns at that point simultaneously. We begin with the solution at time step n and compute the residual $\mathbf{r} = \mathbf{L}(\mathbf{u}^n) - \mathbf{f}(\mathbf{u}^n)$. As $\mathbf{r} \to \mathbf{0}$, $\mathbf{u}^n \to \mathbf{u}^{n+1}$ and our numerical system $\mathbf{L}(\mathbf{u}^{n+1}) = \mathbf{f}(\mathbf{u}^n)$ is satisfied. A 1-dimensional example is shown in figure 3.3. To do this we generate the $D \times D$

Jacobian matrix $\mathbf{J}$ whose elements are

$$J_{ij} = \frac{\partial F_i}{\partial u_j}. \tag{3.42}$$

The adjustment $\delta\mathbf{u}^{(k)}$ to the temporary solution $\mathbf{u}^{(k)}$ is the solution to the linear system

$$\mathbf{J}\,\delta\mathbf{u}^{(k)} = \mathbf{r}. \tag{3.43}$$

The next iteration of the temporary solution is

$$\mathbf{u}^{(k+1)} = \mathbf{u}^{(k)} - \delta\mathbf{u}^{(k)}. \tag{3.44}$$

This continues until the l_2-norm of the residual is within some tolerance near 0. For linear problems the residual can be driven to zero in 1 step.

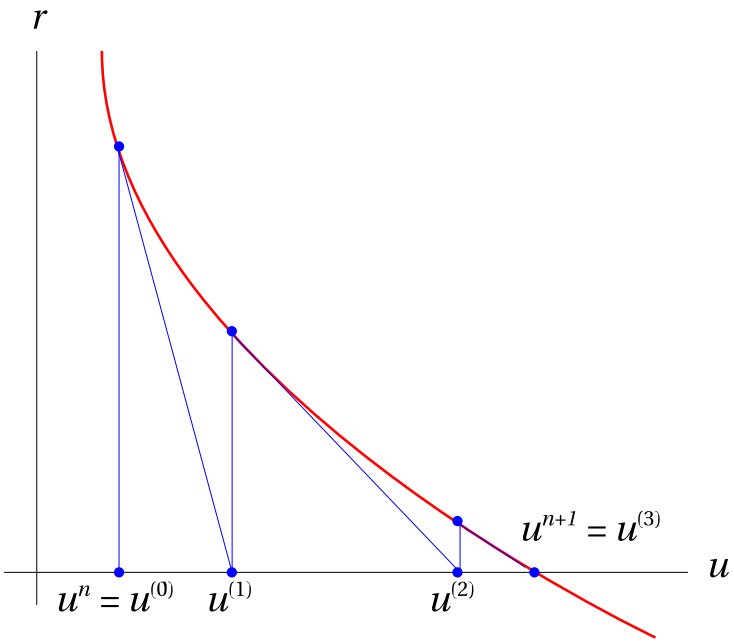

Figure 3.3: Schematic of 1-dimensional Newton Gauss-Seidel method. It begins with an initial guess of the solution (the previous time-step) and the residual $r = L(u^{(k)}) - f(u^n)$ is computed. Find the slope at this point and calculate the next iteration of the solution $u^{(k+1)}$ until r it is sufficiently close to zero.

Chapter 4

Results

The equilibrium solutions from the system (2.1) can be approximated by

$$a(0,x,y) = a_e(0)\text{sech}^2(x/\epsilon_0), \quad h(0,x,y) = h_e(0)\text{sech}^2(x/\epsilon_0) \tag{4.1}$$

allowing for any instability to take effect. Three examples that vary in the parmeter D_0 are detailed below.

For $D_0 = 15.0$, it was shown in [2] that from the stability analysis that there is an unstable breakup mode of $\epsilon_0 m = 0.623$ with an eigenvalue $\lambda_0 = 0.186$ on a domain $[-1,1] \times [0,2]$. This predicts a pattern of $N = m/\epsilon_0 \approx 8$ spots. The domain here is $[-0.5, 0.5] \times [0,1]$ and the numerical simulation in figure 4.1 shows 4 interior spots with half spots at the boundaries.

For $D_0 = 7.6$, there is no breakup instability predicted but rather a zigzag mode of $\epsilon_0 m = 0.315$ with an eigenvalue $\lambda_0 = 0.035$ on a domain $[-1,1] \times [0,2]$. Our numerical simulation in figure 4.2 shows 7 interior spots with half spots at the boundaries. Noteably, the lesser diffusivity of the inhibitor compared to case 1 above allows the spots to exist in closer proximity to each other.

For $D_0 = 6.8$, there is no equilibrium stripe solution. The same behaviour as above dominates the simulation as shown in figure 4.3. The trend towards greater density continues in this case.

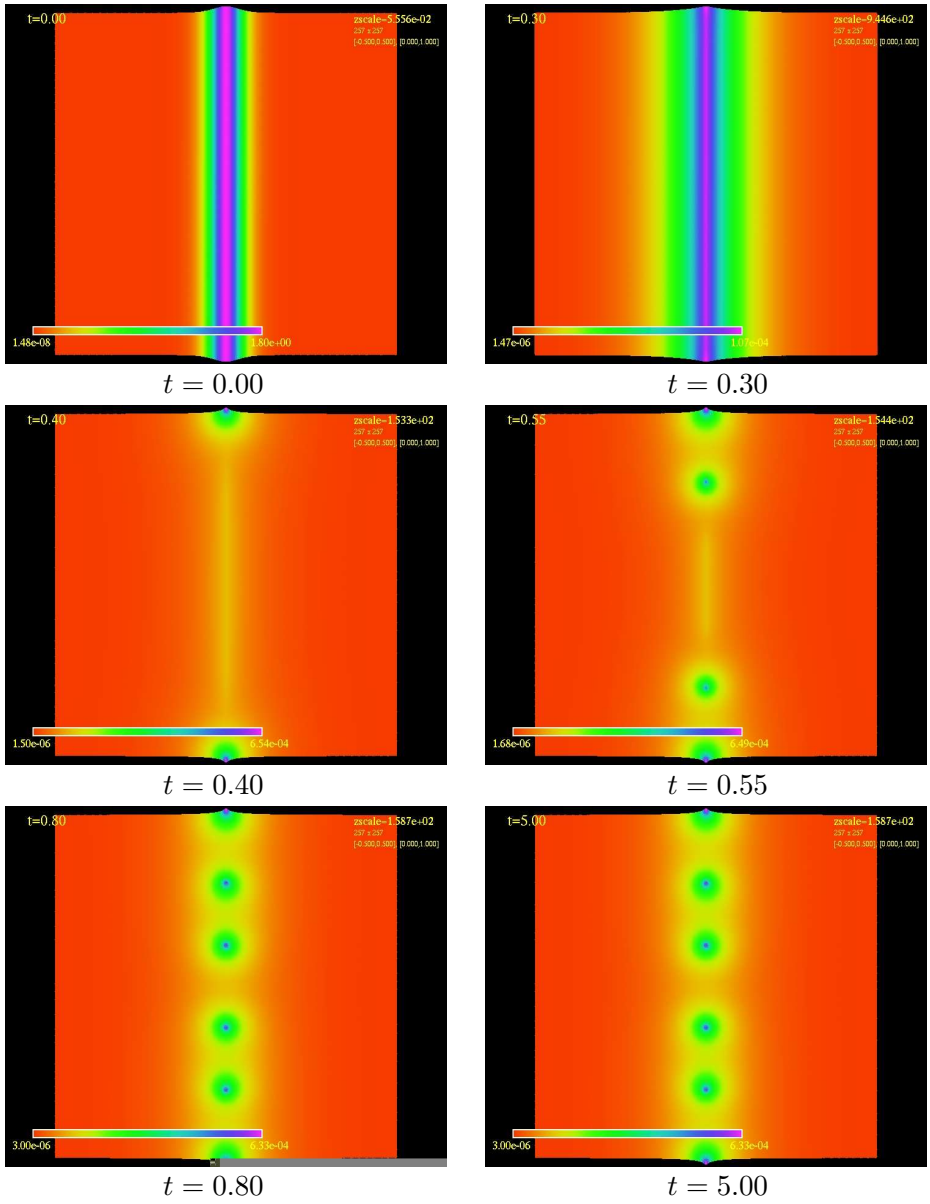

Figure 4.1: Simulation with homoclinic stripe initial conditions for $D_0 = 15.0$, $\epsilon_0 = 0.025$, $\tau = 0.01$, $(p, q, r, s) = (2, 1, 2, 0)$, $a_e(0) = 2.3$, and $h_e(0) = 1.8$. The stripe localizes along the y-axis and breaks up into spots. The pattern seemingly becomes stable beyond this.

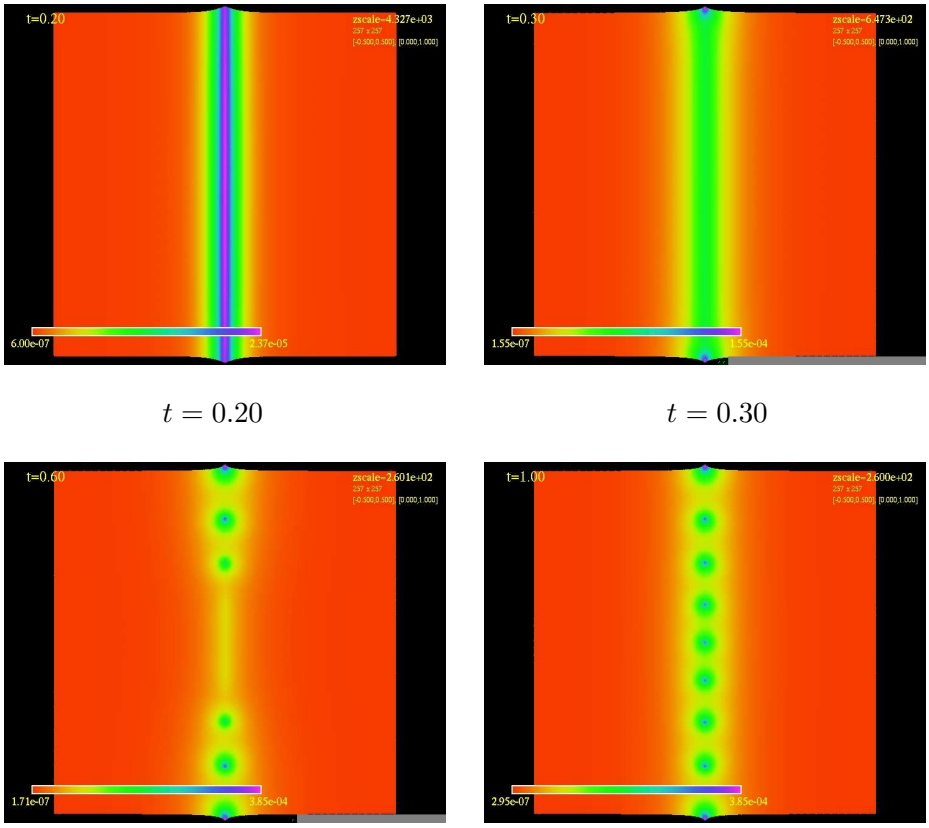

$t = 0.20$ $t = 0.30$

$t = 0.60$ $t = 1.00$

Figure 4.2: Simulation with homoclinic stripe initial conditions for $D_0 = 7.6$, $\epsilon_0 = 0.025$, $\tau = 0.01$, $(p, q, r, s) = (2, 1, 2, 0)$, $a_e(0) = 1.69$, and $h_e(0) = 1.45$. The stripe localizes along the y-axis and breaks up into spots. A greater number of spots form along the center line in comparison to the higher diffusivity $D_0 = 15.0$.

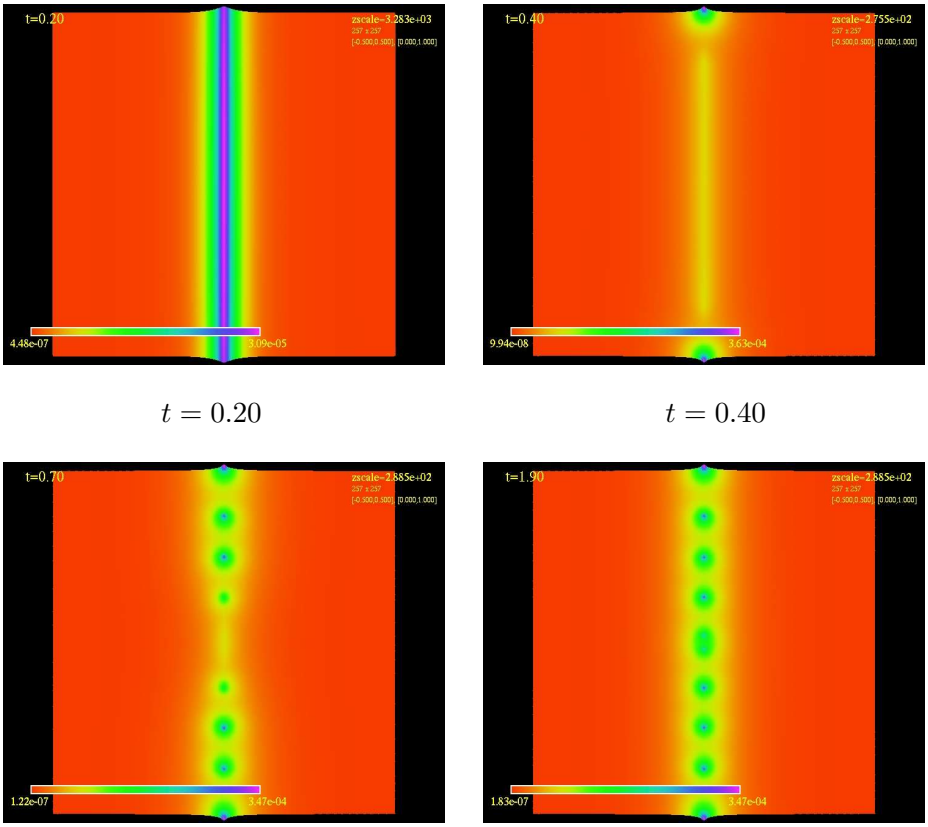

$t = 0.20$ $t = 0.40$

$t = 0.70$ $t = 1.90$

Figure 4.3: Simulation with homoclinic stripe initial conditions for $D_0 = 6.8$, $\epsilon_0 = 0.025$, $\tau = 0.01$, $(p, q, r, s) = (2, 1, 2, 0)$, $a_e(0) = 1.6$, and $h_e(0) = 1.4$. With a slightly lower diffusivity than the case in figure 4.2, an additional spot begins to form at the center.

Chapter 5

Discussion

A Crank-Nicholson, multigrid code was built to solve a two component reaction-diffusion equation in (2+1) dimensions. Homoclinic stripe initial conditions were analyzed for breakup and zigzag instabilities. No zigzag instabilities were demonstrated in the numerical simulations, but breakup patterns showed a spot density dependence on the relative diffusion rates of the two components.

Necessary refinements to the analysis should first include parallization of the code to be run on a cluster to facilitate higher resolution solutions. The qualitative behaviour of the solutions was erratic at low-resolution and only found to be convergent on domains of $N \geq 256^2$ points. Nonlinear systems generally make such demands. Furthermore, a independent residual test was not completed in this work which might display a significantly different behaviour. If the two schemes are shown not to be consistent with each other, the overall results of one or both are called into question.

Other possibilities for exploration of the code are different exponent sets for the reaction kinetics, other initial conditions, or systems with three or more components to model more realistic scenarios in nature.

Bibliography

[1] M.W̃. Choptuik. Finite-difference solutions of partial differential equations [lecture notes], 1997.

[2] T. Kolokolnikov, W. Sun, M. J. Ward, and J. Wei. The stability of a stripe for the gierer-meinhardt model and the effect of saturation. 2005.

[3] H. M. Martinez. *J. Theor. Biol.*, 36, 1972.

[4] H. Meinhardt. *Models of Biological Pattern Formation.* Academic Press, London, 1982.

[5] A. Turing. Phil. trans. roy. soc. B 237, 1952.